

# The Orbit of X Per and Its Neutron Star Companion

Hugo Delgado-Marti, Alan M. Levine, Eric Pfahl, & Saul A. Rappaport

*Department of Physics and Center for Space Research, Massachusetts Institute of Technology, Cambridge, MA 02139; aml@space.mit.edu*

## ABSTRACT

We have observed the Be/X-ray pulsar binary system X Per/4U 0352+30 on 61 occasions spanning an interval of 600 days with the PCA instrument on board the *Rossi X-ray Timing Explorer (RXTE)*. Pulse timing analyses of the 837-s pulsations yield strong evidence for the presence of orbital Doppler delays. We confirm the Doppler delays by using measurements made with the All-Sky Monitor on *RXTE*. We infer that the orbit is characterized by a period  $P_{orb} = 250$  d, a projected semimajor axis of the neutron star  $a_x \sin i = 454$  lt-s, a mass function  $f(M) = 1.61 M_\odot$ , and a modest eccentricity  $e = 0.11$ . The measured orbital parameters, together with the known properties of the classical Be star X Per, imply a semimajor axis  $a = 2.2$  AU, and an orbital inclination  $i \sim 23^\circ$ – $30^\circ$ .

We discuss the formation of the system in the context of the standard evolutionary scenario for Be/X-ray binaries. The orbital eccentricity just after the supernova explosion was almost certainly virtually the same as at present, because the Be star is much smaller than the orbital separation. We find that the system most likely formed from a pair of massive progenitor stars, and probably involved a quasi-stable and nearly conservative transfer of mass from the primary to the secondary. We find that the He star remnant of the primary most likely had a mass  $\lesssim 6 M_\odot$  after mass transfer. If the supernova explosion was completely symmetric, then the present orbital eccentricity indicates that  $\lesssim 4 M_\odot$  was ejected from the binary. If, on the other hand, the birth of the neutron star was accompanied by a “kick” of the type often inferred from the velocity distribution of isolated radio pulsars, then the resultant orbital eccentricity would likely have been substantially larger than 0.11. We have carried out a Monte Carlo study of the effects of such natal kicks, and find that there is less than a 1% probability of a system like that of X Per forming with an orbital eccentricity  $e \lesssim 0.11$ . Finally, we speculate that there may be a substantial population of neutron stars formed with little or no kick.

*Subject headings:* Stars:individual (X Per) — stars:individual (4U 0352+30) — stars:neutron — X-rays:stars — supernovae:supernova explosions — supernovae:kick velocities

## 1. INTRODUCTION

X Per is a bright and highly variable star with a visual magnitude that ranges from  $\sim 6.1$  to  $\sim 6.8$  (Mook et al. 1974, Roche et al. 1997). When the star is particularly bright, its spectrum displays strong emission in  $H\alpha$  and other Balmer lines which marks this clearly as a Be-type system; when the star is faint, the emission lines disappear and it appears to be a normal early-type star (Fabregat et al. 1992, Roche et al. 1997 and references therein). The variability is commonly supposed to be caused by the formation and dissipation of a disk around the star, as in other Be stars, and appears to require free-free and free-bound emission within the disk in addition to electron scattering of the photospheric flux (e.g., Kunjaya & Hirata 1995, Telting et al. 1998). The spectral class of the underlying OB star has been estimated to be O9.5 III to B0 V (Slettebak 1982, Fabregat et al. 1992, Lyubimkov et al. 1997). Based on spectroscopic parallax, distance estimates range from  $700 \pm 300$  pc up to  $1.3 \pm 0.4$  kpc (Fabregat et al. 1992, Lyubimkov et al. 1997, Roche et al. 1997, Telting et al. 1998). Lyubimkov et al. (1997) have used both spectroscopic and photometric observations of the low-luminosity diskless phase of X Per to infer the characteristics of the visible component; their results indicate that X Per is likely to have a mass of  $\sim 13\text{--}20 M_{\odot}$  and a radius of  $5\text{--}10 R_{\odot}$ .

X Per is also the optical counterpart of the low-luminosity X-ray source 4U 0352+30 (Braes & Miley 1972, van den Bergh 1972). X-ray observations have, furthermore, revealed pulsations with a period of  $\sim 835$  s (White et al. 1976). This indicates that X Per must be a binary system containing both a Be star and either a slowly rotating neutron star or a white dwarf. For the first 5 years after the discovery of pulsations, the pulsar exhibited apparently erratic pulse frequency variations superposed on a long-term trend in which it was spinning up at the rate of  $\dot{P}_{\text{pulse}}/P_{\text{pulse}} = -1.5 \times 10^{-4} \text{ yr}^{-1}$ . This was followed by  $\sim 20$  years of spindown at a similar absolute rate (White et al. 1976, Robba et al. 1996, Di Salvo et al. 1998 and references therein). In all, there have been only about two dozen determinations of the pulse period of 4U 0352+30, so that its pulse period behavior on short timescales (e.g., weeks, months, and even a year) is not well documented. The X-ray luminosity varies on long timescales (years) from as high as  $\sim 3 \times 10^{35} \text{ ergs s}^{-1}$  to as low as its current value of

$\sim 5 \times 10^{34} \text{ ergs s}^{-1}$  (for an assumed distance of 1.3 kpc; Roche et al. 1993; also see Di Salvo et al. 1998).

The observed pulse period variations strongly suggest that the X-ray source is an accreting neutron star, with the period variations largely due to accretion torques (see, e.g., Bildsten et al. 1997 and references therein). White et al. (1982) have argued that considerations of the X-ray luminosity and spectrum in the context of accretion from a stellar wind strongly indicate that 4U 0352+30 is a neutron star. Haberl et al. (1998) have noted that the 837 second rotation period is one of the longest known for any neutron star.

The only report of an orbital period for X Per ( $\sim 580$  days) was given by Hutchings et al. (1974) and was based on optical spectroscopy (also see Hutchings, Crampton, & Redman 1975, Hutchings 1977). Penrod & Vogt (1985) explained the radial velocity results reported by these authors by emission variably filling in the Balmer absorption lines, so that the apparent radial velocity curve did not represent the velocity of X Per. This cast doubt on the interpretation of  $\sim 580$  days as the orbital period. Moreover, this period has never been securely confirmed by any subsequent optical or X-ray observations (Weiskopf et al. 1984, Reynolds et al. 1992, Roche et al. 1993, Smith & Roche 1999). There have been other suggestions of orbital periods based on weak evidence. In retrospect, one of the most interesting of these was a possible  $\sim 250$  d periodicity in pulse period measurements noticed by White et al. (1982).

There is one line of evidence that qualitatively supports the idea of a long orbital period for X Per, viz. the “Corbet diagram” (Corbet 1986, van den Heuvel & Rappaport 1987) in which the pulse period is plotted versus orbital period for the known accretion powered X-ray pulsars. For the  $\sim 10$  systems containing Be stars there is a good correlation between pulse period and orbital period which can be represented by the relation

$$P_{\text{orb}} \sim 18(P_{\text{pulse}}/1 \text{ s})^{2/5} \text{ days} \quad (1)$$

with a residual scatter of about a factor of two. For a pulse period of 837 s, eq. (1) predicts an orbital period of  $\sim 266$  d.

We have observed 4U 0352+30 with the Proportional Counter Array (PCA) on the *Rossi X-ray Timing Explorer (RXTE)* in order to track the pulse phase of the neutron star over a substantial interval of time and to thereby allow us to search for a Doppler

signature of orbital motion. We have also utilized observations of 4U 0352+30 made with the *RXTE* All-Sky Monitor (ASM) in our search. In Section 2 we describe the *RXTE* observations, and provide a log of observation dates, durations, and pulse arrival times. The pulse timing analysis of the PCA data and the results which indicate an orbit with a period of 250 days are described in Section 3. In Section 4 we examine the possibility that the observed pulse arrival time delays arose from a random walk in the pulse phase due to accretion torques, and conclude that this is quite unlikely. In this section, we also present the results of our successful search for orbital Doppler delays in observations made with the ASM. The astrophysical implications of a wide yet only mildly eccentric orbit in a Be star X-ray binary are discussed in the context of binary evolution scenarios and natal neutron star kicks in Section 5.

## 2. OBSERVATIONS

Observations of X Per (4U 0352+30) have been carried out with the PCA and HEXTE instruments on *RXTE* over an interval of 600 days. Each observation typically spans about 7000 seconds ( $\sim 8.5$  pulse periods), with a  $\sim 2000$  sec gap due to Earth occultations. The first few observations were performed at approximately 2 day intervals. The interval between later observations was gradually increased to about 2 weeks after one year, with the exception of a  $\sim 62$  d interval with no observations when the Sun passed through the nearby region of the sky. The observations continued past the first year with a nearly constant spacing of about 2 weeks. Most recently, data were acquired at intervals of three weeks. A log of the observations is given in Table 1. The data acquired from the PCA were telemetered in “Goodxenon1” and “Goodxenon2” modes which preserve the 1 microsecond time resolution and the inherent energy resolution of the detectors.

The count rates from 4 of the 61 PCA observations of 4U 0352+30 are shown in Figure 1. The individual 837-s pulsations are clearly evident, although there is significant structure from pulse to pulse as well as on shorter timescales. The variability exhibited in Figure 1 is typical of all the observations.

The All-Sky Monitor (Levine et al. 1996) onboard *RXTE* has obtained some 21,000 intensity measurements of 4U 0352+30 over the past 4 years. Each measurement is an average over an interval of 90 s,

which is sufficiently short to allow the possibility of observing the 837-s pulsations. The mean count rate in the ASM of 4U 0352+30 is  $0.69 \text{ s}^{-1}$ , and the mean value of the signal to noise ratio of individual observations is only  $\sim 0.7$ . Nonetheless, the large number of observations allows meaningful results to be obtained.

Background-subtracted count rates averaged over time intervals of  $\sim 5000$  s or more, as seen in both the PCA and ASM, are shown in Figure 2 for the entire 4 year interval covered by the observations. There are no obvious trends or periodic variations in the source intensity as seen by either instrument. A quantitative analysis of temporal variability using these intensity data is presented in Section 4.3.

## 3. ANALYSIS AND RESULTS

The 2–20 keV band count rate data from each of the PCA observations were folded modulo a trial pulse period, after the observation times were adjusted to the Solar System barycenter. Each folded pulse profile was then cross correlated with a pulse template to find a pulse arrival time for that observation. In practice, this procedure was iterated to improve the pulse template by averaging phase-aligned profiles from individual observations. Details of this procedure can be found in many references (e.g., Levine, Rappaport, & Zojcheski 2000). The 61 barycentric pulse arrival times are given in Table 1.

Background-subtracted pulse profiles in several energy bands are shown in Figure 3; the 2–20 keV profile was used for the template. The pulse profile has a shape that is somewhere between triangular and sinusoidal, with a modulation fraction of about 50% (peak-to-peak amplitude divided by the mean). We have found that the basic shape of the pulse profile did not vary over the course of the PCA observations, nor did it depend significantly on energy band within the range 2–20 keV.

In Figure 4 we show the results of making different assumptions about the number of pulses that occurred between each of our measured arrival times. For each sequential pair of pulse arrival times, we divided the time interval by the number of pulses,  $n$ , we believe occurred between the two arrival times to obtain an average pulse period for the interval. We also show the pulse periods that would be deduced if the cycle count had been  $n + 3$ ,  $n + 2$ ,  $n + 1$ ,  $n - 1$ ,  $n - 2$ , or  $n - 3$ . In any plausible accretion torque scenario for this neutron star (see the discussion below),

the pulse period cannot have changed by more than a fraction of a second over an interval of 600 days. Therefore, the plot shows that the pulse period must be close to 837.5 s and that the pulse count between observations is generally unambiguously determined. The only interval in which the correct pulse count is not obvious from Figure 4 is the long gap in the observations between day 298 and day 360. Below, we discuss evidence obtained from a detailed coherent analysis of the pulse arrival times that indicates that we have correctly determined the pulse count in this long interval. The pulse numbers that we believe to be correct are listed in Table 1.

Once pulse numbers have been assigned to the arrival times, we can subtract off the best fitting constant pulse period, and examine the residual pulse arrival time delays. The result is shown in the top panel of Figure 5. There are clear delays as large as approximately plus and minus a full pulse period. We next fit a model including constant, linear, and quadratic terms to the pulse arrival times to simulate a simple spin up or spin down of the neutron star. The residuals with respect to this simple model are shown in the lower panel of Figure 5; they suggest orbital motion with a period of  $\sim 250$  days.

We next carried out a formal search for best-fitting Keplerian orbits. Models of both circular and mildly eccentric orbits were fit to the arrival times. The circular orbit fits included 5 parameters to be determined, i.e., constant, linear, and quadratic terms to model the pulsar spin and terms proportional to  $\sin \omega_{orb} t$  and  $\cos \omega_{orb} t$  to account for orbital Doppler delays. In searching for eccentric orbit solutions, we utilized the approximation wherein small eccentricities produce sinusoidal modulations in the pulse arrival times at twice the orbital frequency. The small orbital eccentricities found (see the discussion below) justify this approximation. Therefore, our eccentric orbit fits included terms proportional to  $\sin 2\omega_{orb} t$  and  $\cos 2\omega_{orb} t$  as well as the 5 terms used in the circular orbit fits. The circular and eccentric orbit fits were each repeated for closely spaced values of the orbital period in the range 30 to 600 days.

A plot of the magnitude of the root-mean-square (rms) pulse arrival time fit residuals vs. orbital period for circular and mildly eccentric orbits is shown in Figure 6. This figure shows that there are clearly defined best-fit solutions at orbital periods very close to 250 days.

The pulse arrival time delays are shown together

with the best-fit circular and eccentric orbit models in Figure 7. For this figure the constant, linear, and quadratic terms of each fit have been subtracted from both the arrival times and the models. The circular orbit has a period of 249.9 days, while the eccentric orbit fit yields a period of 250.3 days, with a corresponding eccentricity of  $0.111 \pm 0.018$  ( $1\sigma$  confidence). The orbital parameters are summarized in Table 2. The statistical uncertainties in the orbital parameters were determined by using the rms residuals from the best fit as a measure of the uncertainty in the individual pulse arrival times. The eccentric orbit fit yields an rms scatter about the fit of 21.8 s, compared with 27.7 s for the circular orbit fit. We interpret this difference as being significant at the  $\sim 6\sigma$  level. We found that the effects of any correlation of the other parameters with the orbital period were small; the  $1\sigma$  error estimates in Table 2 did not need to be adjusted for this effect.

Earlier we noted that determination of the pulse count during the long gap in the observations required a more detailed analysis. We have therefore carried out orbital fits under the assumption that the number of pulses in the gap was one more or less than we assumed for the analysis given above. Neither case yielded a fit with an rms value less than 79 s for any orbital period in the range 30 to 350 d (see Fig. 6). Both cases could thus be ruled out with high confidence.

The value of the pulse period derivative that we derive from the best fitting circular and eccentric orbits is  $\dot{P}_{pulse}/P_{pulse} = 1.26 \pm 0.01 \times 10^{-4} \text{ yr}^{-1}$  (see Table 2). The positive derivative indicates that the neutron star is spinning *down*. This is consistent with the long-term pulse period changes observed in X Per over the past  $\sim 20$  years.

The orbital parameters discussed above for X Per yield a mass function of  $1.61 \pm 0.05 M_{\odot}$  (see Table 2). If we assume that the mass of X Per is in the range of  $15\text{--}30 M_{\odot}$ , and that the neutron star has a mass of  $1.4 M_{\odot}$ , then the orbital inclination lies in the range of  $23^{\circ}\text{--}30^{\circ}$ . In turn, this implies that the semimajor axis of the orbit is about 2.2 AU in size.

## 4. ATTEMPTS TO VERIFY THE ORBIT

### 4.1. Simulations with Random Walk in Pulse Phase

Since a number of X-ray pulsars exhibit spinup as well as spindown episodes on a wide range of

timescales (e.g., Bildsten et al. 1997), it is worth asking whether the sinusoidal component of the variation of the pulse arrival time delays of 4U 0352+30 could be due to variations in the intrinsic pulsar spin rate instead of orbital motion. We therefore carried out simulations of a model of intrinsic spin rate variations to test this alternate hypothesis. The model we selected, that of random white torque noise, while hardly unique, can at least test the plausibility that the observed pulse arrival time delays could be generated by torques on the neutron star (see, e.g., Deeter et al. 1989). For these simulations, we generated artificial sets of pulse arrival times corresponding to a set of observations covering a 600-day interval, and spaced in a manner roughly approximating that of the *RXTE* observations. For each simulated data set, a string of 6000 Gaussian-distributed random numbers was generated to represent the values of the torque averaged over 0.1 day time intervals. The amplitude of the Gaussian random noise was set so as to produce, after many such simulations, an *rms* value of  $\dot{P}_{pulse}/P_{pulse} = 1.2 \times 10^{-4} \text{ yr}^{-1}$  over the 600-d time interval. The simulated time series of accretion torque noise was then integrated twice in succession in order to obtain its effect on pulse phase as a function of time.

Each simulated data set was analyzed in the same way as the actual *RXTE* data, i.e., we tested a range of trial orbital periods and, for each one, carried out a five parameter fit which included constant, linear, and quadratic terms, as well as orbital amplitude and phase. The best fitting “orbital solution” was selected from among the various trial orbital periods, subject to the constraint that the mass function exceed a minimum value, i.e.,  $f(M) > 0.14 M_{\odot}$ . This constraint eliminates solutions with implausible values of the mass function. In particular, if we assume that the stellar masses are  $12 M_{\odot}$  and  $1.4 M_{\odot}$ , then  $f(M) > 0.14 M_{\odot}$  for 97% of randomly chosen orientations of the orbital plane. If the mass of the optical star is greater than  $12 M_{\odot}$ , then it is even less likely that the mass function would violate this constraint.

The rms deviation of the simulated measurements from the best fit, the corresponding mass function, and the corresponding orbital period were obtained for each of  $10^4$  simulations. For about 30% of these, there was no solution for any orbital period in the range 30 to 600 days with  $f(M) > 0.14 M_{\odot}$ . Most of the remaining  $\sim 70\%$  have best-fit orbital periods near 600 days, i.e., commensurate with the length of the

simulated data train. The results for the  $\sim 45\%$  of the simulations that satisfy the mass function constraint and for which the best-fit orbital period  $P_{orb} < 600$  d are summarized in Figure 8, where projections of three combinations of the parameters are shown. If we restrict the “acceptable fits” to those with orbital periods  $< 350$  days, a value both comfortably longer than 250 days and shorter than the length of the simulated data train, then only 6.2% of the original simulations fall into this category. If we further require that the fits yield rms deviations less than 30 s, a value just above that for the best circular-orbit fit of the actual PCA timing observations, then only 0.3% of the simulated data sets produce acceptable results. Finally, if we require that the solutions also have positive values of  $\dot{P}_{pulse}/P_{pulse}$ , then only 0.2% of the simulations are completely “acceptable”. Thus, we conclude that there is only a small chance that a random walk in pulse phase would yield sinusoidally varying pulse arrival time delays similar to those we have observed, and thereby mimic the Doppler delays from a plausible orbit of the neutron star.

#### 4.2. Pulse Timing Analysis of *RXTE* ASM Data

The intensities measured with the ASM were Fourier transformed after the observation times were adjusted to the Solar System barycenter. The resultant power density spectrum (PDS) is shown in Figure 9a for periods in the vicinity of the 837-s pulse period; the average power has been normalized to unity. Note that there is a statistically significant group of small peaks with powers exceeding  $\sim 8$  and covering the period range of 837.3 to 838.0 s. The observation times were then further adjusted to remove the effects of an assumed constant spin-down of the X-ray pulsar with a rate of  $\dot{P}_{pulse}/P_{pulse} = 1.56 \times 10^{-4} \text{ yr}^{-1}$  (see Table 3). The PDS of the data set with this correction is shown in Figure 9b. The power is now more concentrated in a narrow region centered around a period of 837.3 s, with several peaks exceeding 15. Finally, we corrected the observation times to remove the time delays due to the eccentric orbit derived from the PCA analysis (see Table 2). The results in Figure 9c now show a sharp peak (of height 76) at 837.33 sec, which is just the expected pulse period for the start of the ASM epoch  $\sim 2.5$  yr earlier than the start of the PCA observations.

Given this clear detection of the pulsations in the ASM data, we decided to utilize these data to inde-

pendently determine the orbital parameters. To accomplish this, each of the parameters  $P_{orb}$ ,  $a_x \sin i$ ,  $T_{\pi/2}$ ,  $e$ , and  $\dot{P}_{pulse}$ , was varied systematically over a wide range while the others were fixed at values determined either in the PCA analysis or earlier in this procedure. For each set of the parameter values, the ASM observation times (corrected to the Solar System barycenter) were adjusted to remove the effects of pulsar spin down and orbital motion so as to attempt to obtain coherence in the 837-s pulsations. Each adjusted set of data was subjected to a Fourier analysis. We then searched all the PDSs made while varying a particular parameter to find the largest value of the power, and to thereby establish a value for that parameter. Each of the parameters was varied in turn until the best values for all were obtained. Note that the pulse frequency was effectively varied since we searched an extended frequency range ( $858^{-1}$  -  $770^{-1}$  Hz) of each PDS. Rough estimates of the uncertainties in the parameter values were established by finding the ranges of parameter values that yielded maximum powers of at least  $[P_{max}^{1/2} - (1/2)^{1/2}]^2$ , where  $P_{max}$  is the largest power in any of the transforms.

The orbital parameter determinations from the ASM data were carried out for each of three separate sets: (i) data from MJD 50087 to 50995 (i.e., prior to the PCA observations), (ii) data from MJD 50995 to 51535 (i.e., contemporaneous with the PCA observation interval), and (iii) all the ASM data. The best fit parameters and their  $1\sigma$  single-parameter confidence errors are listed in Table 3. Three conclusions can be drawn from these numbers. The first is that the orbital parameter values are clearly consistent with those found from the PCA analysis, though the uncertainties are larger for the ASM results. Second, the value of  $\dot{P}_{pulse}/P_{pulse}$  during the ASM observations which preceded the PCA observations, was significantly larger (by  $\sim 20\%$ ) than during the PCA observation interval. Finally, the existence of the 250-day orbit in X Per is clearly confirmed by the earlier ASM observations which are completely independent of the PCA observations (i.e., different detectors and non-overlapping time intervals).

#### 4.3. Search for Orbital Light Curve in the X-Ray Intensity Data

If the neutron star moved through a stellar wind whose intensity falls off as  $1/r^2$ , then a periodic variation in accretion rate that ranges from  $\dot{M}_0(1 - e)^{-2}$

to  $\dot{M}_0(1 + e)^{-2}$  would be expected from an orbit with a small eccentricity  $e$ , where  $\dot{M}_0$  is the mean accretion rate. We therefore carried out a formal search for sinusoidal variations in intensity as a function of trial orbital period over the range 50 days to 600 days using the data shown in Figure 2. No statistically significant periodicities were found, and  $2\sigma$  upper limits on the amplitudes of such periodicities were set for each trial period; the results are shown in Figure 10. The  $2\sigma$  upper limit on periodic variability (as the amplitude of a sine wave) in the vicinity of  $P_{orb} \sim 250$  d is only 9% of the mean count rate. When this upper limit is interpreted in terms of allowed orbital eccentricities via the above expressions, the  $2\sigma$  upper limit on  $e$  from the X-ray intensity data alone, for orbital periods near 250 days is  $e < 0.04$ . This is clearly inconsistent with the value obtained from the orbital fit of  $e = 0.111 \pm 0.018$ . If, on the other hand, the stellar wind density profile from the Be star falls off more slowly than  $1/r^2$ , the limit that can be obtained from the intensity data alone is weaker, e.g., the limit would be  $e < 0.09$  for a  $1/r$  density profile. Such a value would be marginally consistent with the observed eccentricity. Of course, the interpretation of the lack of X-ray variability, in terms of orbital eccentricity, is based on the Bondi-Hoyle theory of accretion from a stellar wind (Wang 1981, Livio et al. 1986, Ruffert 1999) which must be considered substantially uncertain. For a more extensive discussion of neutron stars in eccentric orbits accreting from winds of Be star companions, see Waters et al. (1988, 1989).

## 5. DISCUSSION

Bildsten et al. (1997) list 5 Be/X-ray binaries with measured orbital parameters. These are shown schematically, but to scale, in Figure 11. For each system, the Be star is fixed, and the orbit of the neutron star is drawn with the *full* semimajor axis  $a$ . To estimate the semimajor axis we utilized the measured *projected* semimajor axis and mass function for the neutron star, and then simply assumed masses for the Be and neutron stars of  $18 M_{\odot}$  and  $1.4 M_{\odot}$ , respectively. Also shown on the figure for comparison is the X Per system.

The average eccentricity for the 5 Be/X-ray binaries other than X Per is  $e = 0.4$ , in sharp contrast with the much smaller value of 0.11 for X Per. This is especially noteworthy in that the X Per system has

the smallest value of  $R_{Be}/a$  ( $\lesssim 0.05$ ), which indicates that there is virtually no chance that the system has circularized significantly since the birth of the neutron star (see, e.g., Zahn 1977, Zahn 1989, Verbunt & Phinney 1995, Soker 1998). Here we take  $20 R_{\odot}$  as the upper limit on the radius of the Be star. Thus, for any plausible circularization time for such a Be star filling its Roche lobe (e.g., a few thousand yr), the tidal circularization timescale, which is proportional to  $(a/R)^8$ , in the widely separated X Per system would exceed the lifetime of X Per by orders of magnitude.

If we assume that the orbit of X Per has an eccentricity of 0.11 which has remained unchanged since the birth of the neutron star, then we can set interesting and potentially important constraints on the dynamics of the supernova explosion and the mass that was ejected from the binary system. First, however, we consider the origin of the X Per/4U0352+30 system. In the conventional scenario for forming a Be X-ray binary (Rappaport & van den Heuvel 1982, van den Heuvel & Rappaport 1987, Habets 1987), the more massive star (e.g.,  $\sim 10\text{--}25 M_{\odot}$ ) in the progenitor binary evolves first and fills its Roche lobe. Depending on the evolutionary state of the primary at the onset of mass transfer (see, e.g., Kippenhahn & Weigert 1967, Podsiadlowski, Joss, & Hsu 1992 and references therein), the Roche lobe overflow of mass onto the secondary may proceed either on a thermal timescale or be dynamically unstable. In the former case, relevant to the formation of Be stars, it is unclear how conservative the mass transfer may be. In general, the orbital separation will first decrease, and then, if conditions are right (see below), increase until the mass transfer terminates.

In this scenario, detailed binary evolution calculations are required to determine how much envelope mass is retained by the He core of the original primary star (see, e.g., Podsiadlowski et al. 1992). However, simple orbital dynamics provide an analytic relation among the final orbital separation, the initial separation, and the final and initial masses of the system (see equation 5 of Podsiadlowski et al. 1992). There are two “free” parameters in this relation, viz.,  $\alpha$ , the specific angular momentum carried away by matter ejected from the binary system in units of the binary angular momentum per reduced mass, and  $\beta$ , the fraction of mass lost by the primary that is retained by the secondary during mass transfer. We plot in Figure 12 some illustrative examples of the ratio of final to

initial orbital separations as a function of fractional mass loss of the primary star for different assumed values of  $\beta$ . The initial stellar masses in this particular example are 15 and  $10 M_{\odot}$ , and we adopted a value  $\alpha = 1.5$  which might be typical for mass lost through the outer Lagrange points. (We remind the reader that in the above paragraph as well as in the next paragraph the words “initial” and “final” refer only to the process of quasi-conservative mass transfer from the primary to the secondary *prior* to the supernova.)

As one can see from Figure 12, for conservative mass transfer the final orbit can be substantially larger than the initial orbit. However, for  $\beta \lesssim 0.6$  the orbit tends to shrink dramatically. This is true for a range of plausible initial mass ratios. If the initial orbital separation in the X Per system had been larger than  $\sim 5$  AU, the primary would not have filled its Roche lobe and transferred mass to the secondary (and the system would have become unbound after the supernova). Moreover, the orbit just prior to the supernova explosion was probably not much closer than 2 AU (see Fig. 14 and the associated discussion below). Thus, since the orbit did not shrink by more than a factor of  $\sim 5/2$  during the mass-transfer phase from the primary, we can see from Fig. 12 that  $\beta$  cannot be substantially less than  $\sim 0.6$ . Finally, we conclude that the initial orbital separation of the primordial binary probably could not have been much smaller than about 0.5 AU. This latter conclusion is based upon the fact that in order for the final to initial orbital separation to increase by a factor of  $\sim 4$ , the value of  $\beta$  must be close to unity; then one must also satisfy the condition that the computed current-epoch mass of X Per should not be too large. In summary, we infer that the primordial binary which formed the current X Per system had an initial orbital separation of between 0.5 and 5 AU, experienced quasi-stable Roche-lobe overflow when the primary evolved, and that most of the mass lost by the primary was retained by the secondary.

We now consider the effects on the orbit of the collapse of the Fe core of the remnant primary and the ensuing supernova explosion. First, we examine the case where the supernova explosion was spherically symmetric in the rest frame of the progenitor star, i.e., no kick velocity was imparted to the newly born neutron star. If the orbit of the progenitor of the neutron star and its companion (i.e., the present-day X Per) was circular, and there was no kick imparted to

the neutron star at its birth, then there is a simple relationship among the current orbital eccentricity, the total mass of the progenitor system,  $M_{tot}$  (just before the supernova explosion), and the mass ejected by the explosion,  $\Delta M$ :

$$e = \Delta M / (M_{tot} - \Delta M) \quad (2)$$

Some illustrative examples taken from this relationship are plotted in Figure 13. Here we show the eccentricity induced by the supernova explosion as a function of the mass ejected, for a plausible range of values (10 - 30  $M_{\odot}$ ) for the total mass of the binary just prior to the supernova explosion. Note that for the supernova to have produced an orbital eccentricity  $e < 0.15$  (i.e., the  $2\sigma$  observational upper limit), no more than  $\sim 4 M_{\odot}$  can have been ejected from the system. Thus, we conclude that the progenitor of the neutron star was a He star with mass  $< 5 - 6 M_{\odot}$ . Estimates of the minimum mass of a He star that can produce a neutron star are close to  $2.3 M_{\odot}$  (see, e.g., Habets 1986a, Habets 1986b).

The results shown in Figure 13 are for the case where the neutron star was *not* given a kick when the Fe core of its progenitor star collapsed. However, it is conventional wisdom that most neutron stars are given substantial kicks at their birth (e.g., Lyne & Lorimer 1994, Cordes & Chernoff 1997, Cordes & Chernoff 1998, Fryer, Burrows, & Benz 1998, Hansen & Phinney 1997). The measured 3-dimensional space velocity distribution for isolated neutron stars is uncertain, but is generally characterized by a function with a mean speed of  $\sim 300 \text{ km s}^{-1}$  and which tends to vanish at low speeds. There seems to be a growing consensus that these large space velocities result from natal kicks to the neutron star, and that the “slingshot” effect from neutron stars born in binary systems is insufficient to produce the observed velocities (see, e.g., Cordes & Chernoff 1997, 1998; Fryer, Burrows, & Benz 1998; Hansen & Phinney 1997; cf. Iben & Tutukov 1996). The small observed eccentricity in X Per seems to be qualitatively at odds with this “universal” kick distribution.

In order to study the problem more quantitatively, we have carried out a modest Monte Carlo study of supernovae in binary systems of the type that are directly relevant to the formation of 4U 0352+30/X Per. We considered circular orbits for the progenitor He star and its massive companion (the current X Per). We chose the mass of the He star to be  $6 M_{\odot}$ . For more massive He stars even a no-kick supernova

explosion would leave the orbit more eccentric than is observed – unless the supernova kick fortuitously “corrects” the eccentricity that would otherwise be induced. We take the mass of the companion star to be  $18 M_{\odot}$ , which is approximately the current mass of X Per. We also considered 4 different initial orbital separations for the pre-supernova binary: 0.5, 1, 2, and 4 AU. For each Monte Carlo case we chose at random a kick speed from a Maxwellian distribution (Hansen & Phinney 1997):

$$p(v) = \sqrt{\frac{\pi}{2}} \frac{v^2}{v_0^3} e^{-v^2/2v_0^2}, \quad (3)$$

while the direction of the kick was chosen from an isotropic distribution (see, e.g., Brandt & Podsiadlowski 1995). In this expression we adopted a value for  $v_0$  of  $190 \text{ km s}^{-1}$  which yields a mean kick velocity of  $320 \text{ km s}^{-1}$  (Hansen & Phinney 1997). These quantities then uniquely determine the final post-supernova orbital parameters; these were recorded for each system. For each separation this procedure was repeated  $10^6$  times, and the distributions of the results are shown in Figure 14. We find that  $\sim 3\text{-}24\%$  of the binaries remain bound following the supernova explosion, with the exact percentage depending sensitively on the pre-supernova semimajor axis. The best match to the current orbital period of 250 days is an initial orbital separation of 2 AU. However, as can readily be seen from the distribution of eccentricities, there is only a *very small* probability of finding the post-supernova orbit with an eccentricity of  $\lesssim 0.11$ ; typically  $\sim 1\%$  of the binaries which remain bound have an eccentricity this small.

From our analysis it seems reasonable to conclude that, at least for the X Per binary, the Be/neutron star pair formed via a completely unremarkable scenario. Because of the small eccentricity in the system, however, our Monte Carlo kick study clearly indicates that it is unlikely that a substantial kick was imparted to the neutron star at birth. However, one should be cautious about drawing far reaching conclusions based on this one system. We point out that there are at least two other relatively wide X-ray binaries that may exhibit a similarly small orbital eccentricity: 2S 1553–54 and GS 0834–43 (see Bildsten et al. 1997 and references therein). The orbit of the transient X-ray source 2S 1553–54 was determined on only one occasion during a single orbital cycle (Kelley, Rappaport, & Ayasli 1983). The system was found to have a period of 29 days and an eccentricity  $e < 0.09$  ( $2\sigma$



limit). The companion star has never been optically identified. Nonetheless this system seems like another reasonable candidate for a Be/X-ray binary with only a small eccentricity. The transient source GS 0834–43 (Wilson et al. 1997) was found to have an orbital period of 106 days, but the orbital parameters were not uniquely determined due to effects of accretion torque noise. However, the best fitting solutions yield an orbital eccentricity of  $\sim 0.17$ . The optical counterpart of GS 0834–43 has recently been identified with a Be star (Israel et al. 2000).

While it is always conceivable that this system was produced via a highly improbable event, it seems more reasonable in the case of X Per to draw the conclusion that not all neutron stars receive kicks of a magnitude consistent with the Hansen & Phinney (1997) distribution of single pulsar velocities. Therefore we adopt the somewhat unconventional view that perhaps a substantial fraction of all neutron stars do *not* suffer significant kicks at birth (see also Iben & Tutukov 1996, Cordes & Chernoff 1998).

This work was supported in part by NASA Grants NAG5-7479, NAG5-4057, and NAG5-8368, and Contract NAS5-30612. We are grateful to Jean Swank and Evan Smith for support in conducting the *RXTE* observations.

## REFERENCES

- Bildsten, L., et al. 1997, *ApJS*, 113, 367
- Braes, L. L. E., & Miley, G. K. 1972, *Nature*, 235, 273
- Brandt, N., & Podsiadlowski, P. 1995, *MNRAS*, 274, 461
- Corbet, R. H. D. 1986, *MNRAS*, 220, 1047
- Cordes, J. M., & Chernoff, D. F. 1997, *ApJ*, 482, 971
- Cordes, J. M., & Chernoff, D. F. 1998, *ApJ*, 505, 315
- Deeter, J. E., Boynton, P. E., Lamb, F. K., & Zylstra, G. 1989, *ApJ*, 336, 376
- Di Salvo, T., Burderi, L., Robba, N. R., & Guainazzi, M. 1998, *ApJ*, 509, 897
- Fabregat, J., et al. 1992, *A&A*, 259, 522
- Fryer, C., Burrows, A., & Benz, W. 1998, *ApJ*, 496, 333
- Haberl, F., Angelini, L., Motch, C., & White, N. E. 1998, *A&A*, 330, 189
- Habets, G. M. H. J. 1986a, *A&A*, 165, 95
- Habets, G. M. H. J. 1986b, *A&A*, 167, 61
- Habets, G. M. H. J. 1987, *A&A*, 184, 209
- Hansen, B. M. S., & Phinney, E. S. 1997, *MNRAS*, 291, 569
- Hutchings, J. B. 1977, *MNRAS*, 181, 619
- Hutchings, J. B., Cowley, A. P., Crampton, D., & Redman, R. O. 1974, *ApJ*, 191, L101
- Hutchings, J. B., Crampton, D., & Redman, R. O. 1975, *MNRAS*, 170, 313
- Iben, I., & Tutukov, A. V. 1996, *ApJ*, 456, 738
- Israel, G. L., et al. 2000, *MNRAS*, in press (astro-ph/0001085)
- Kelley, R. L., Rappaport, S., & Ayasli, S. 1983, *ApJ*, 274, 765
- Kippenhahn, R., & Weigert, A. 1967, *Z. Astrophys.*, 65, 251
- Kunjaya, C., & Hirata, R. 1995, *PASJ*, 47, 589
- Levine, A. M., Bradt, H., Cui, W., Jernigan, J. G., Morgan, E. H., Remillard, R., Shirey, R. E., & Smith, D. A. 1996, *ApJ*, 469, L33
- Levine, A. M., Rappaport, S., & Zojcheski, G. 2000, submitted to *ApJ*(astro-ph/9911173)
- Livio, M., Soker, N., de Kool, M., & Savonije, G. J. 1986, *MNRAS*, 222, 235
- Lyne, A. G., & Lorimer, D. R. 1994, *Nature*, 369, 127
- Lyubimkov, L. S., Rostopchin, S. I., Roche, P., & Tarasov, A. E. 1997, *MNRAS*, 286, 549
- Mook, D. E., Boley, F. I., Foltz, C. B., & Westpfahl, D. 1974, *PASP*, 86, 894
- Penrod, G. D., & Vogt, S. S. 1985, *ApJ*, 299, 653
- Podsiadlowski, Ph., Joss, P. C., & Hsu, J. J. L. 1992, *ApJ*, 391, 246

- Rappaport, S. & van den Heuvel, E. P. J. 1982, in Proceedings of IAU Symposium No. 98 on Be Stars, eds. M. Jasek & H. G. Groth (Dordrecht: Reidel), 327
- Reynolds, A. P., Hilditch, R. W., Bell, S. A., Pollacco, D. L., & Edwin, R. P. 1992, MNRAS, 258, 439
- Robba, N. R., Burderi, L., Wynn, G. A., Warwick, R. S., & Murakami, T. 1996, ApJ, 472, 341
- Roche, P., et al. 1993, A&A, 270, 122
- Roche, P., et al. 1997, A&A, 322, 139
- Ruffert, M. 1999, A&A, 346, 861
- Slettebak, A. 1982, ApJS, 50, 55
- Smith, M. A., & Roche, P. 1999, ApJ, 522, 444
- Soker, N. 1998, ApJ, 496, 833
- Telting, J. H., Waters, L. B. F. M., Roche, P., Boogert, A. C. A., Clark, J. S., de Martino, D., & Persi, P. 1998, MNRAS, 296, 785
- van den Bergh, S. 1972, Nature, 235, 273
- van den Heuvel, E. P. J., & Rappaport, S. 1987, in IAU Colloquium No. 92, Physics of Be Stars, eds. A. Slettebak and T. D. Snow (Cambridge University Press), 291
- Verbunt, F., & Phinney, E. S. 1995, A&A, 296, 709
- Wang, Y.-M. 1981, A&A, 102, 36
- Waters, L. B. F. M., de Martino, D., Habets, G. M. H. J., & Taylor, A. R. 1989, A&A, 223, 207
- Waters, L. B. F. M., Taylor, A. R., van den Heuvel, E. P. J., Habets, G. M. H. J., & Persi, P. 1988, A&A, 198, 200
- Weiskopf, M. C., et al. 1984, ApJ, 278, 711
- White, N. E., Mason, K. O., Sanford, P. W., & Mordin, P. 1976, MNRAS, 176, 201
- White, N. E., Swank, J. H., Holt, S. S., & Parmar, A. N. 1982, ApJ, 263, 277
- Wilson, C. A., Finger, M. H., Harmon, B. A., Scott, D. M., Wilson, R. B., Bildsten, L., Chakrabarty, D., & Prince, T. A. 1997, ApJ, 479, 388
- Zahn, J-P. 1977, A&A, 57, 383; erratum 67, 162.
- Zahn, J-P. 1989, A&A, 220, 112

TABLE 1  
JOURNAL OF OBSERVATIONS

Start Time (MJD <sup>c</sup> )	Duration (s)	Exposure (s)	Count Rate <sup>a</sup> (cts s <sup>-1</sup> PCU <sup>-1</sup> )	Pulse Arrival Time <sup>b</sup> (s)	Pulse Number
50995.033	7648	4960	34.4	0	0
50996.651	7472	5088	32.1	139033	166
50998.846	7631	5056	25.1	329189	393
51000.897	3327	3328	24.1	505881	604
51002.963	6944	4464	34.5	684357	817
51005.925	11056	6256	28.7	940623	1123
51008.031	8255	5648	28.7	1122409	1340
51011.030	7231	4912	25.3	1382033	1650
51014.775	8191	5360	31.8	1705366	2036
51018.774	7232	4544	27.8	2050419	2448
51021.829	7712	5520	26.0	2315078	2764
51025.831	7344	5296	24.8	2660167	3176
51029.998	6864	4448	27.4	3020347	3606
51034.769	6928	4944	33.6	3432402	4098
51039.799	7023	4864	35.6	3867102	4617
51044.805	10176	5328	26.5	4300151	5134
51049.706	7664	5264	28.8	4723142	5639
51054.652	7696	4864	24.2	5150307	6149
51060.839	7295	4907	47.0	5685524	6788
51066.506	8352	4832	35.1	6174684	7372
51072.704	7296	5136	14.4	6710771	8012
51079.372	7936	3936	22.4	7286185	8699
51085.645	7424	5488	31.9	7828195	9346
51092.540	6847	4592	34.5	8423815	10057
51099.711	8127	5440	33.7	9043673	10797
51107.576	7583	4832	23.4	9723109	11608
51115.594	7567	5152	34.8	10415978	12435
51122.445	8415	5488	31.0	11008235	13142
51131.502	7231	4880	33.4	11790789	14076
51139.718	8431	5184	37.4	12500405	14923
51147.714	8542	5408	33.4	13191633	15748
51154.436	7583	5200	23.5	13772213	16441
51166.297	8654	5343	24.9	14796872	17664
51174.626	7167	4880	30.4	15516615	18523
51185.287	7711	4896	36.0	16437345	19622
51194.221	7663	4960	25.8	17209750	20544
51204.417	8078	5375	33.1	18090212	21595
51214.344	7231	4912	29.2	18948065	22619
51225.268	8014	5664	26.9	19892186	23746
51236.063	8414	4768	22.8	20824568	24859
51247.267	6510	4480	28.1	21792933	26015
51258.118	7182	4896	34.4	22730264	27134
51269.310	7518	4880	34.2	23696849	28288
51281.164	8014	5808	24.0	24721370	29511
51292.888	6767	3360	43.4	25734120	30720

TABLE 1—*Continued*

Start Time (MJD <sup>c</sup> )	Duration (s)	Exposure (s)	Count Rate <sup>a</sup> (cts s <sup>-1</sup> PCU <sup>-1</sup> )	Pulse Arrival Time <sup>b</sup> (s)	Pulse Number
51355.004	6847	4640	20.9	31101333	37127
51367.899	7344	4896	26.4	32214823	38456
51377.888	7279	4976	27.3	33077855	39486
51392.937	3727	3712	32.0	34378244	41038
51406.007	8608	5328	27.1	35507717	42386
51420.662	7776	5288	44.7	36773788	43897
51433.721	9760	5154	34.5	37902423	45244
51447.614	8739	6258	22.1	39102200	46676
51463.877	8448	5244	23.7	40508074	48354
51478.579	7543	5130	22.6	41778194	49870
51492.622	8139	5958	24.8	42991263	51318
51512.878	19414	5165	25.1	44741312	53407
51534.688	8378	5778	35.7	46626158	55657
51556.300	8439	5838	24.2	48493430	57886
51576.474	7838	4939	27.8	50236005	59966
51597.240	7726	5306	38.4	52030604	62108

<sup>a</sup>Average count rate for the energy band 2-20 keV

<sup>b</sup>At the Solar System barycenter referenced to 1998 July 1 0:33:6 TDB

<sup>c</sup>Modified Julian Date = Julian Date - 2,400,000.5

TABLE 2  
ORBITAL AND PULSE PARAMETERS

Parameter	Circular Orbit Fit	Eccentric Orbit Fit
$P_{orb}$ (days)	$249.9 \pm 0.5$	$250.3 \pm 0.6$
$a_x \sin i$ (lt-s)	$454 \pm 5$	$454 \pm 4$
$f(M)$ ( $M_\odot$ )	$1.61 \pm 0.06$	$1.61 \pm 0.05$
$T_{\pi/2}$ (MJD)	$51215.5 \pm 0.5$	$51215.1 \pm 0.4$
$P_{pulse}$ (s) <sup>a</sup>	$837.6713 \pm 0.0003$	$837.6712 \pm 0.0003$
$\dot{P}_{pulse}/P_{pulse}$ (yr <sup>-1</sup> )	$(1.26 \pm 0.01) \times 10^{-4}$	$(1.26 \pm 0.01) \times 10^{-4}$
$e$	...	$0.111 \pm 0.018$
$\omega_{peri}$ ( $^\circ$ )	...	$288 \pm 9$
$T_{peri}$ (MJD)	...	$51353 \pm 7$
RMS Scatter (s)	27.7	21.8
$a_0$ <sup>b</sup>	...	31055.6017
$a_1$ <sup>b</sup>	...	$1.1936637 \times 10^{-3}$
$a_2$ <sup>b</sup>	...	$-2.388 \times 10^{-15}$

<sup>a</sup>The epoch for  $P_{pulse}$  is MJD 51000.0.

<sup>b</sup>The pulse phase at the Solar System barycenter may be obtained from  $\phi = a_0 + a_1 t + a_2 t^2 - \Delta t_{orb}(t)/P_{orb}$  where  $\phi$  is in cycles,  $t$  is the time at the Solar System barycenter in seconds since MJD 51296.12602, and  $\Delta t_{orb}(t)$  is the light travel time delay for the eccentric orbit relative to the X Per system barycenter. The phase is defined so that  $\phi = 0$  at maximum intensity (see Fig. 3).

TABLE 3  
ORBITAL PARAMETERS DETERMINED WITH ASM DATA

Parameter	Pre-PCA Data <sup>a</sup>	Co-PCA Data <sup>b</sup>	All ASM Data <sup>c</sup>
$P_{orb}$ (days)	$250 \pm 3$	$253 \pm 10$	$252 \pm 5$
$a_x \sin i$ (lt-s)	$421 \pm 70$	$385 \pm 108$	$444 \pm 66$
$T_{\pi/2}$ (MJD)	$51213 \pm 6$	$51212 \pm 8$	$51215 \pm 6$
$P_{pulse}$ (s) <sup>d</sup>	$837.654 \pm 0.02$	$837.658 \pm 0.01$	$837.666 \pm 0.01$
$\dot{P}_{pulse}/P_{pulse}$ (yr <sup>-1</sup> )	$(1.57 \pm 0.10) \times 10^{-4}$	$(1.23 \pm 0.08) \times 10^{-4}$	$(1.63 \pm 0.05) \times 10^{-4}$
$e$	...	...	$< 0.3$

<sup>a</sup>Data from time interval MJD 50087 to MJD 50995

<sup>b</sup>Data from time interval MJD 50995 to MJD 51535

<sup>c</sup>Data from time interval MJD 50087 to MJD 51535

<sup>d</sup>The epoch for  $P_{pulse}$  is MJD 51000.0.

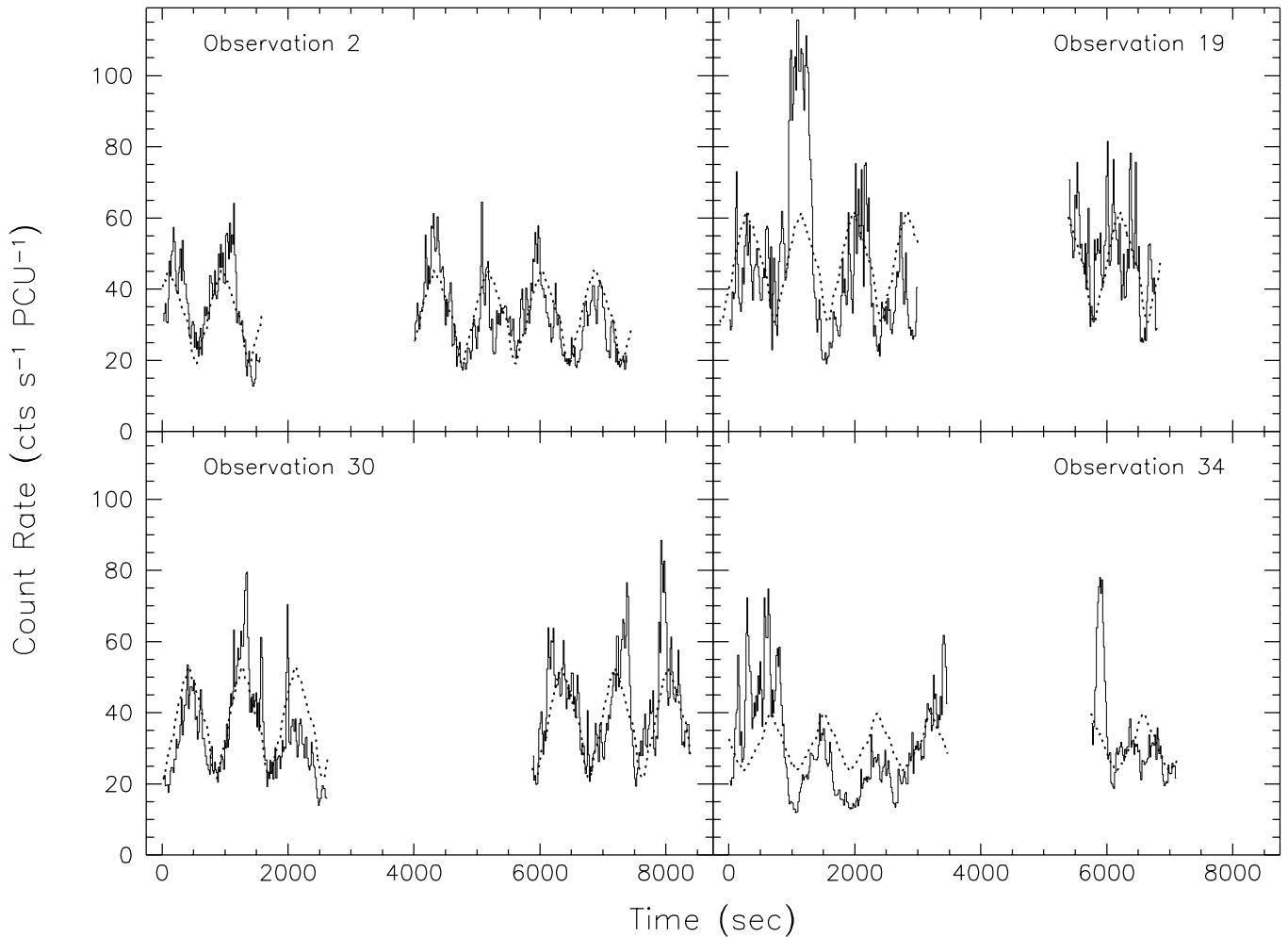


Fig. 1.— Counting rates (2 - 20 keV) during 4 of the 61 PCA observations of 4U 0352+30/X Per. Non-source background has been subtracted. Each observation lasted for typically 7000 s, and was interrupted by a  $\sim 2000$ -s occultation of the source by the Earth. The dashed curves were derived from the average pulse profile (see Figure 2), but a scale factor and additive constant were adjusted for each observation to provide the best fit. These scaled average profiles are meant only to guide the eye and to indicate the degree of variability in the pulsations.

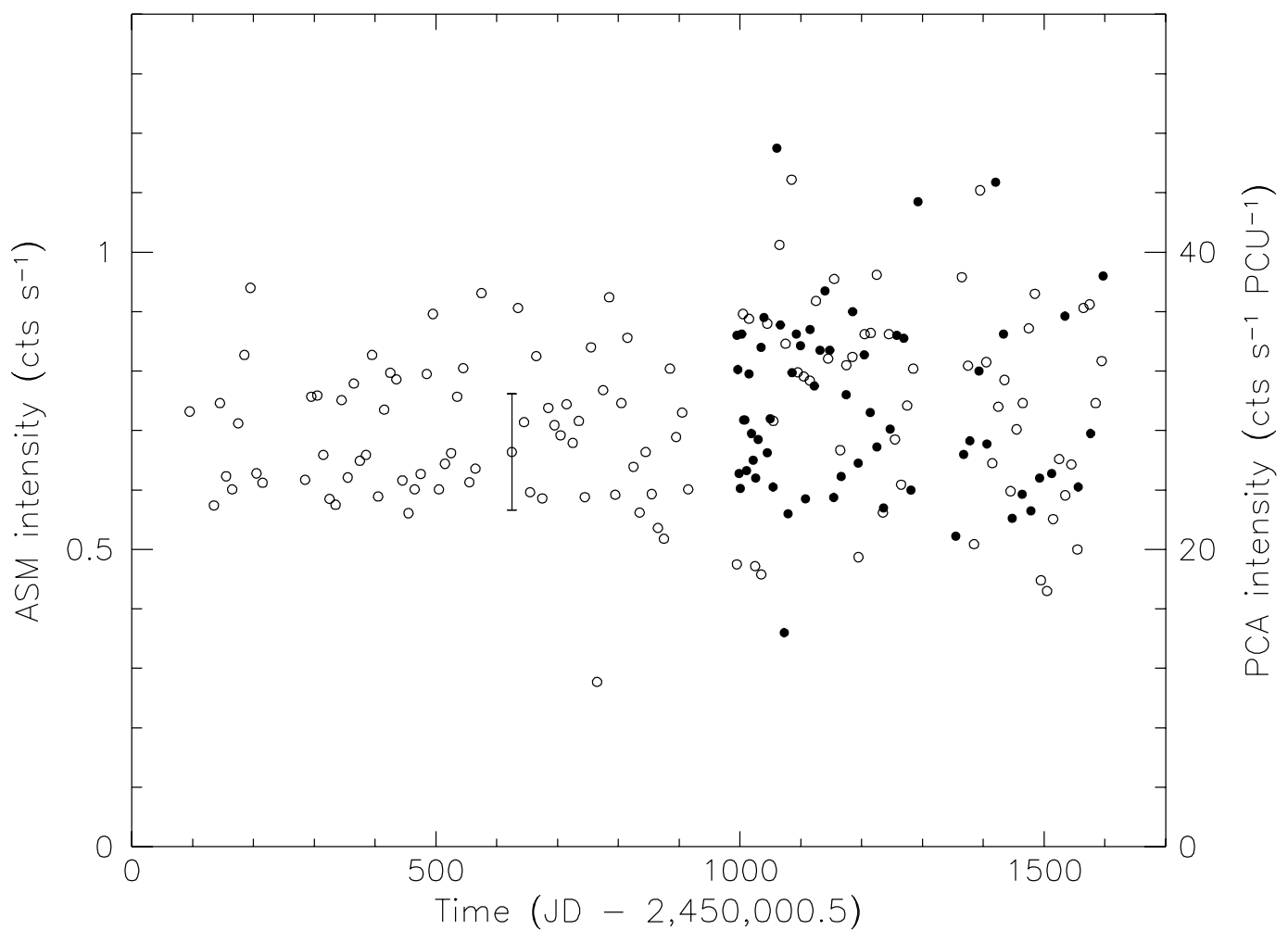


Fig. 2.— X-ray intensity data for 4U 0352+30 over a 4-year interval. The open circles are 10-day averages (2–12 keV) from the ASM (scale on left), while the filled circles are 2–20 keV average background-subtracted count rates from each of the PCA observations (scale on right). A typical  $1\sigma$  uncertainty is shown for one of the ASM intensities. Errors in the average PCA intensities due to counting statistics are negligible.



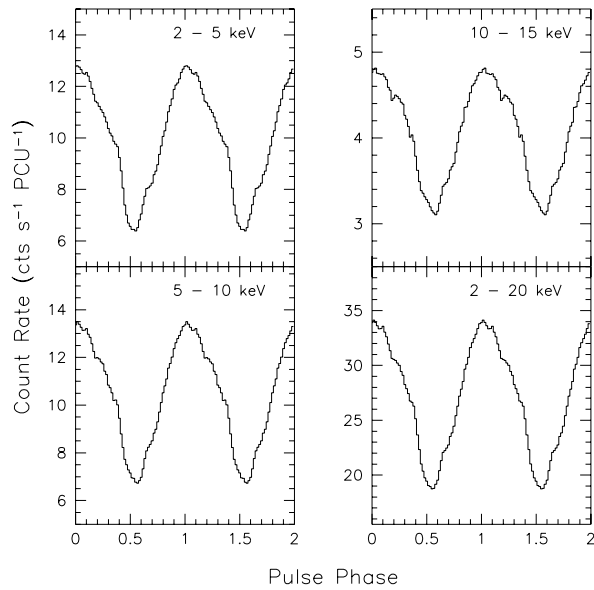


Fig. 3.— Background-subtracted pulse profiles for 4U 0352+30 in 4 energy bands. The profiles are the averages of the phase-aligned pulse profiles from each of the 61 PCA observations. The fluctuations in the profiles due to counting statistics are negligible. Other fluctuations due to the flaring behavior of the source on  $\sim 100$  s time scales may not be negligible.

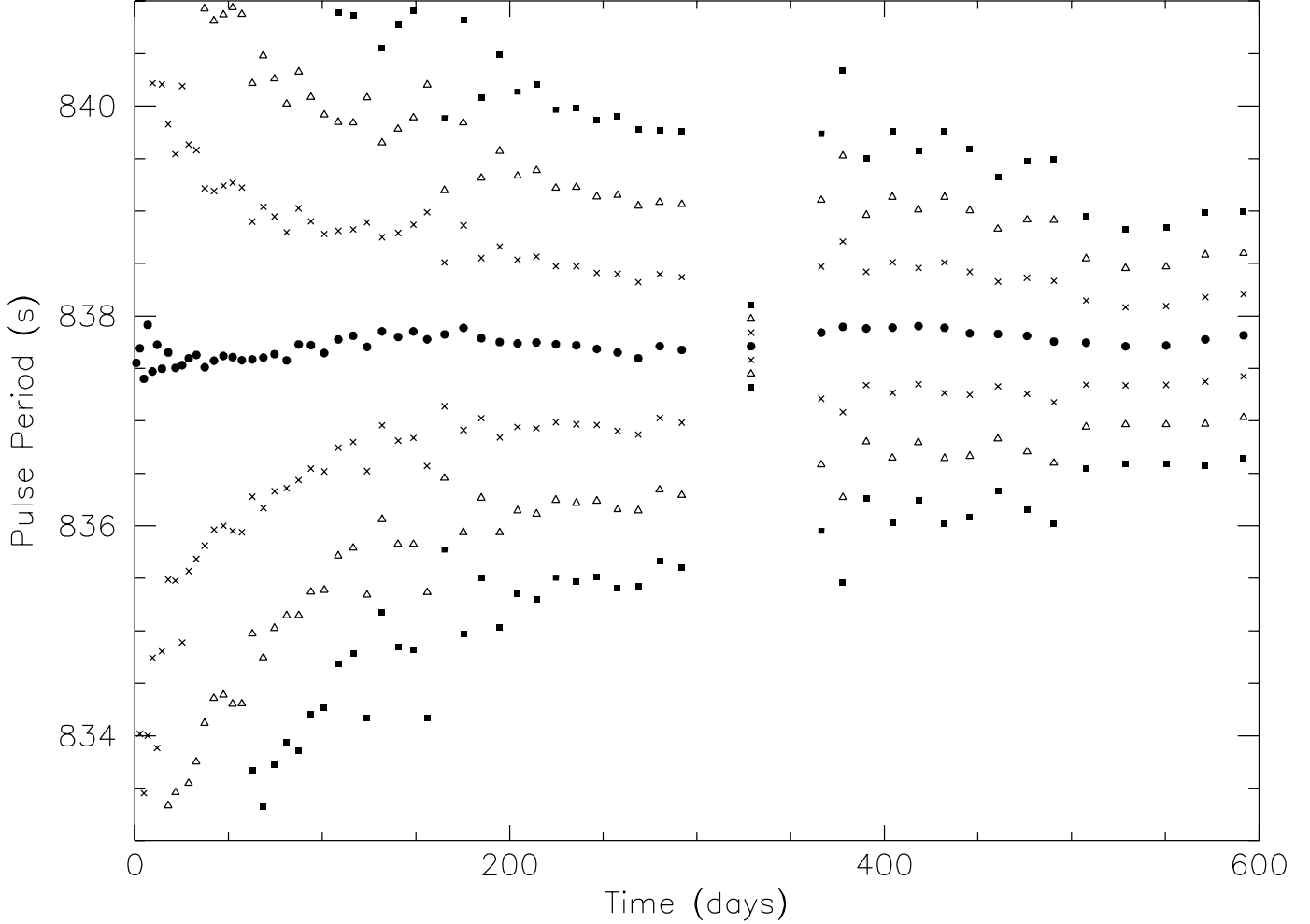


Fig. 4.— Average inter-observation pulse periods for 4U 0352+30. Each pulse period was derived by taking the difference in pulse arrival times between adjacent observations and dividing by an assumed number of pulses between the observations. Pulse periods are shown for seven possible values of the number of pulses between each pair of observations. Only for the assumed pulse numbers that yield the filled circles does the pulse period change slowly and remain within the physically plausible range of  $837.7 \pm 0.5$  s. The only possible ambiguity in pulse number occurs near the large gap in the observations centered near day 330 (see text).

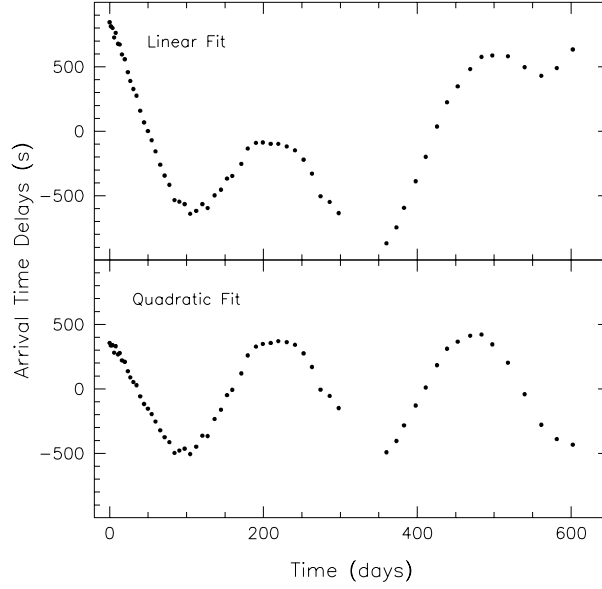


Fig. 5.— Pulse arrival time delays for 4U 0352+30 with respect to the best-fit constant pulse period (top), and with respect to the best-fit quadratic function (bottom).

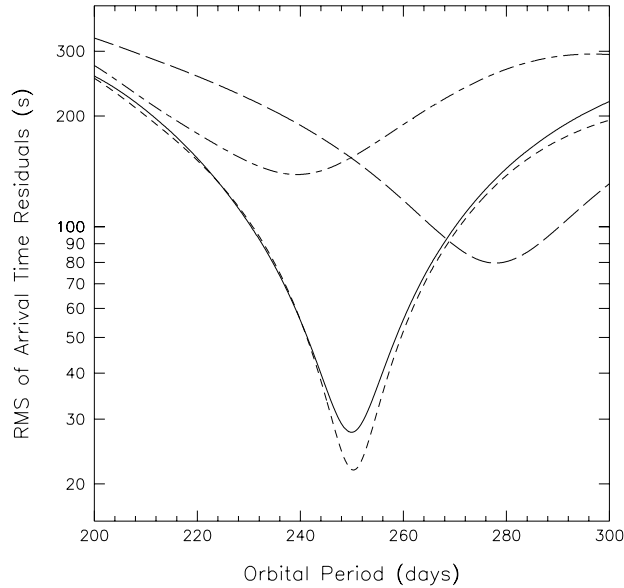


Fig. 6.— RMS residuals from fits of pulse arrival times vs. trial orbital period. The results are shown for the circular orbit fits (solid line), and for mildly eccentric fits with the pulse count in the 62-d gap having three different values, i.e., our nominal count  $n$  (short dashes),  $n + 1$  (long dashes), and  $n - 1$  (short/long dashes). These results confirm that  $n$  is the correct pulse count for the gap. The best fitting orbital period is close to 250 d (see Table 2).

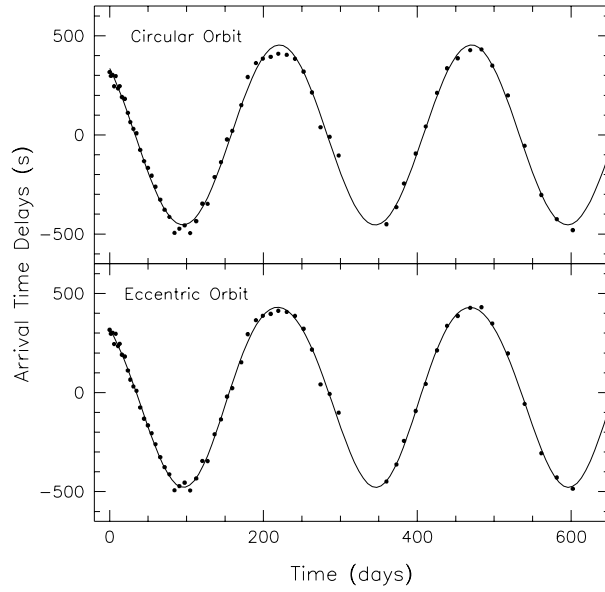


Fig. 7.— Pulse arrival time delays for 4U 0352+30 with fits to a quadratic function plus a circular orbit (top) or a mildly eccentric orbit (bottom). In each case, the best fit quadratic function has been subtracted from the pulse arrival times. The solid curves are the best fit model orbital Doppler delays.

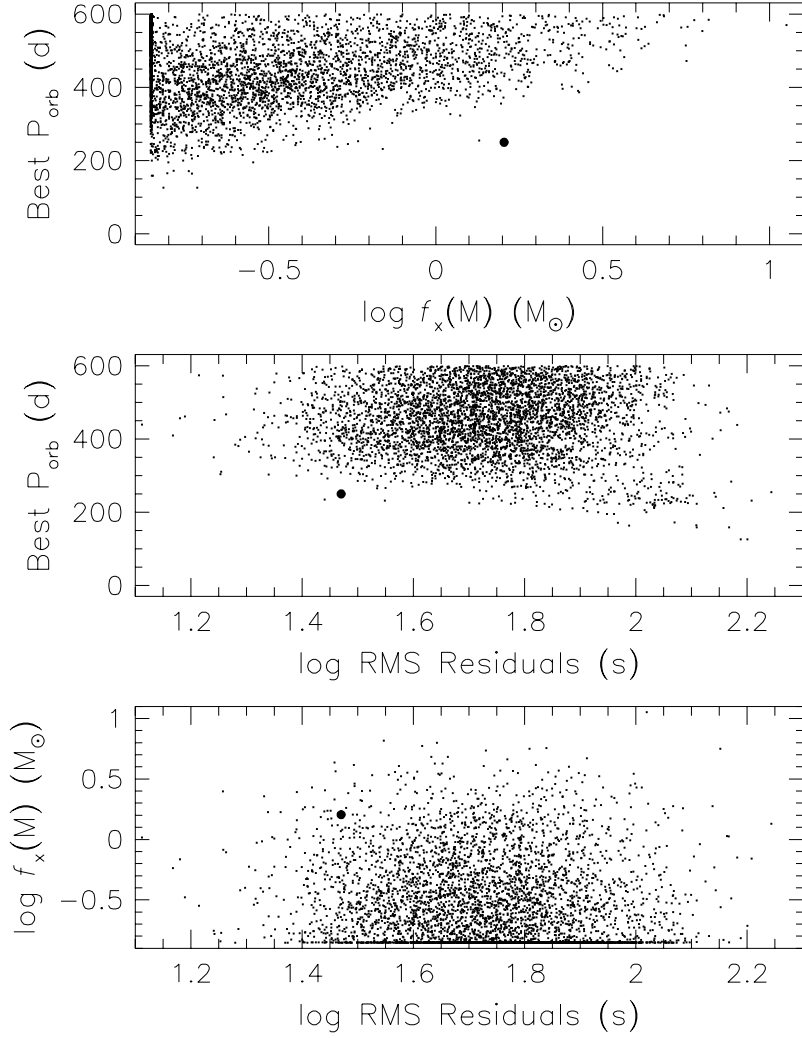


Fig. 8.— Results from  $10^4$  simulations of a pulsar subject to white torque noise. In each panel, each small dot shows the values of two parameters from the best circular-orbit fit to one simulated data set (see text). We only show the dots from the 4490 simulations for which the best fit orbital period was less than 600 days and for which  $f(M) > 0.14 M_{\odot}$ . The large filled circles show the values of the parameters determined from the best circular orbit fit to the actual measurements of 4U 0352+30 (see Table 2).

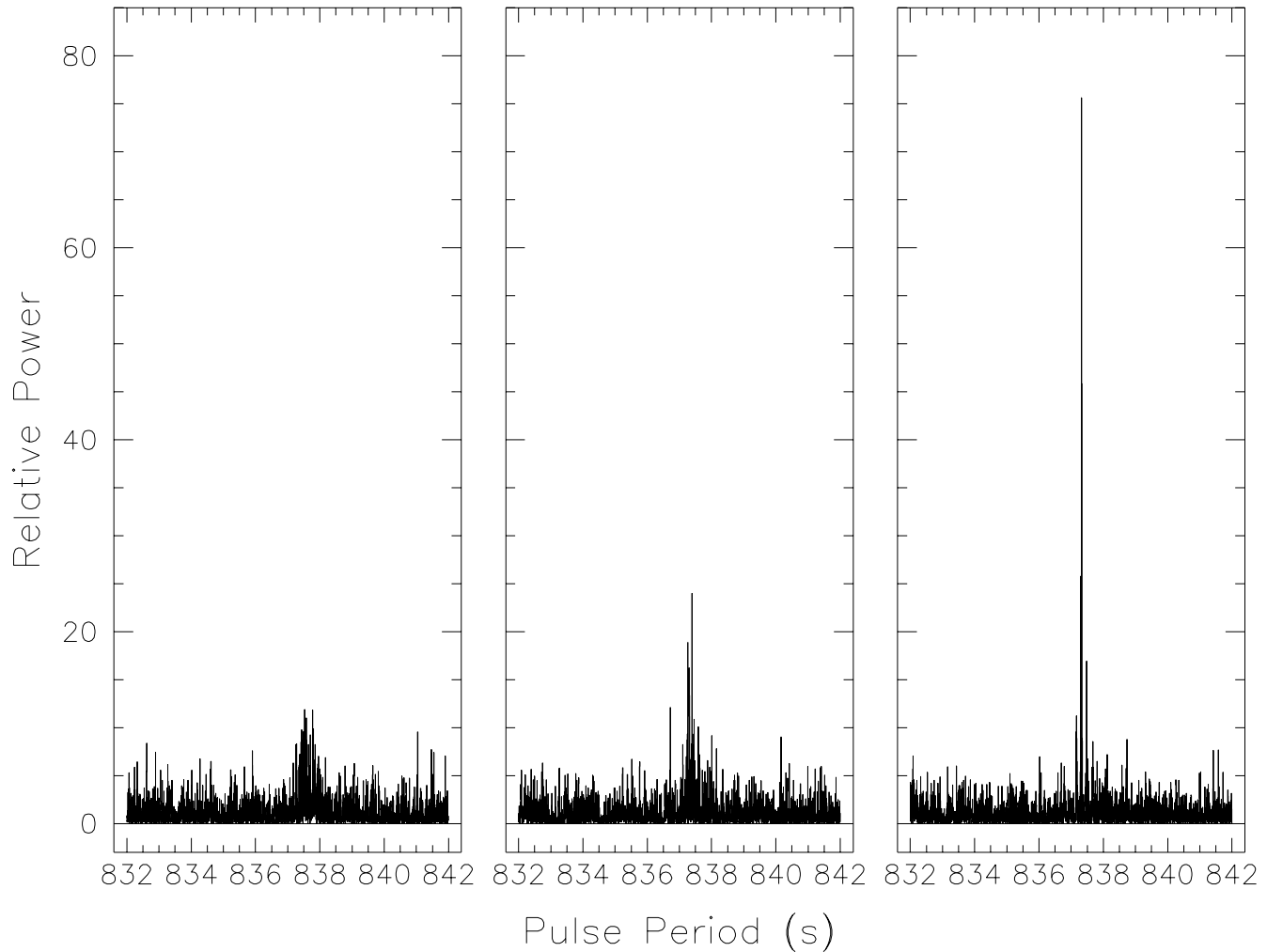


Fig. 9.— Power density spectra (PDSs) computed from data obtained with the ASM. Approximately 21,000 intensity points for 4U 0352+30, obtained over a 4 year interval, were used in the analysis. (left) PDS which results after barycentric corrections were applied to the data. (center) PDS after correcting the times to the barycenter and for a constant value of  $\dot{P}_{pulse}/P_{pulse} = 1.56 \times 10^{-4} \text{ yr}^{-1}$ . (right) PDS after corrections for the eccentric orbit given in Table 2 in addition to the barycentric and pulse period derivative corrections.

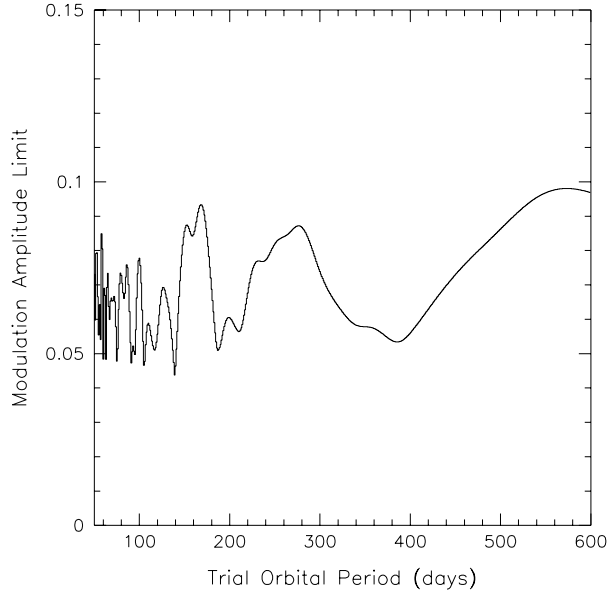


Fig. 10.— Upper limits on sinusoidal variations in the X-ray intensity of 4U 0352+30 derived from the data shown in Figure 2 as a function of trial orbital period. The limits are expressed as fractions of the average intensity and are shown for the  $2\sigma$  confidence level.

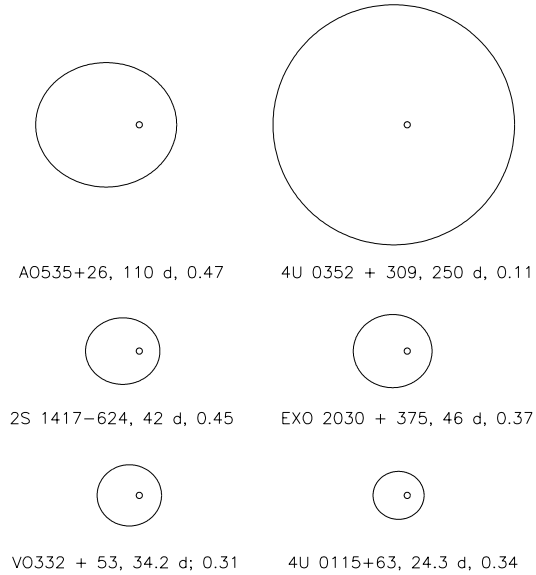


Fig. 11.— Schematic orbits for 6 Be/X-ray binaries drawn to scale (see Bildsten et al. 1997). The orbital period and eccentricity are listed with the source name. The small circle represents the Be star with an illustrative radius of  $10 R_{\odot}$ .

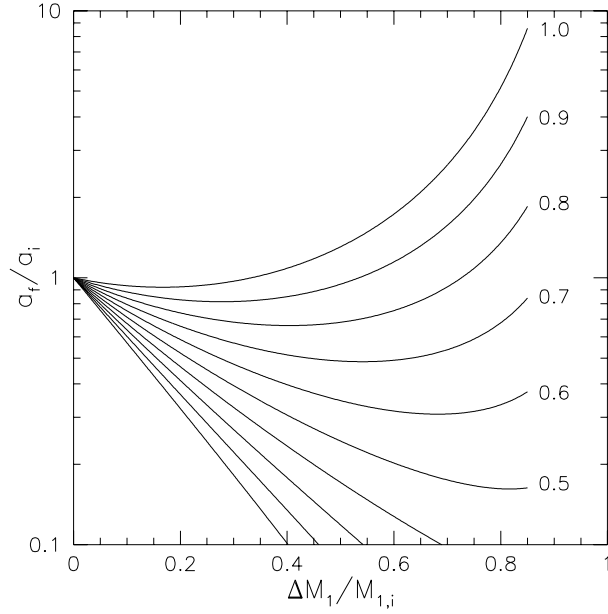


Fig. 12.— Ratio of final to initial pre-supernova orbital separation vs. the fractional mass lost,  $\Delta M_1/M_{1,i}$ , by the primary for the case where a fraction  $\beta$  of mass lost by the primary is retained by the secondary during the Roche-lobe overflow phase (see text). The curves are labelled according to the value of  $\beta$  used in the calculation. The specific angular momentum of the mass ejected from the binary system was taken to be  $1.5a^2\Omega_k$ , where  $a$  and  $\Omega_k$  are the instantaneous values of the orbital separation and Keplerian angular frequency, respectively.

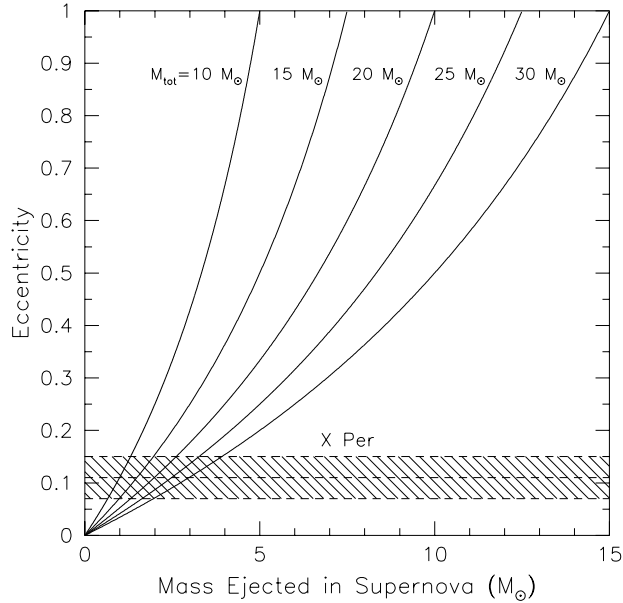


Fig. 13.— The eccentricity induced in binary systems as a function of the mass ejected in a supernova explosion. The calculations are for the case where there is no natal kick imparted to the neutron star. Each curve is labeled with the total mass of the binary system prior to the supernova explosion.



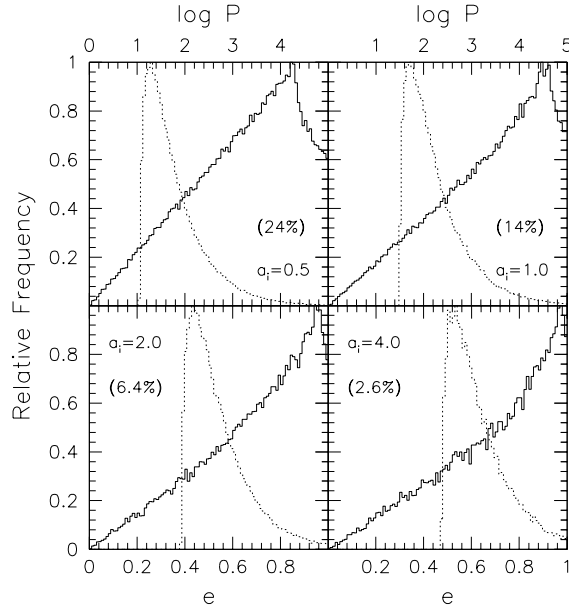


Fig. 14.— Results of a Monte Carlo study of the eccentricities induced in binary systems in which kicks are imparted to the neutron star during the supernova explosion. Each panel shows the results from the simulation of  $10^6$  binary systems with a fixed initial (just before the supernova) orbital separation  $a_i$  (in AU). A kick velocity distribution given by equation (3) was used to select the kicks. The solid (dashed) curves are histograms of the final eccentricity (logarithm of the orbital period in days). The percentage of systems that remain bound after the supernova explosion is also given for each initial separation.